Human muscle stem cell responses to mechanical stress into tunable 3D alginate matrices

Melanie Marquis, Agata Zykwinska, Bruno Novales, Isabelle Leroux, Cindy Schleder, Julien Pichon, Stéphane Cuenot, Karl Rouger

International Journal of Biological Macromolecules 266 (2024) 130823

Contents lists available at ScienceDirect

International Journal of Biological Macromolecules

journal homepage: www.elsevier.com/locate/ijbiomac

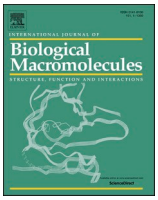

Human muscle stem cell responses to mechanical stress into tunable 3D alginate matrices

Mélanie Marquis [a,*], Agata Zykwinska [b], Bruno Novales [c], Isabelle Leroux [a], Cindy Schleder [a], Julien Pichon [a], Stéphane Cuenot [d], Karl Rouger [a]

[a] Oniris, INRAE, PAnTher, Physiopathologie Animale et bioThérapie du muscle et du système nerveux, 44307 Nantes, France
[b] Ifremer, MASAE, Microbiologie Aliment Santé Environnement, F-44000 Nantes, France
[c] INRAE, BIA, Biopolymères Interactions Assemblages, 44316 Nantes, France
[d] Nantes Université, CNRS, Institut des Matériaux de Nantes Jean Rouxel, IMN, 44322 Nantes cedex 3, France

ARTICLE INFO

Keywords:
Alginate-based hydrogel
Atomic force microscopy
Muscle stem cells

ABSTRACT

Preclinical data acquired for human muscle stem (hMuStem) cells indicate their great repair capacity in the context of muscle injury. However, their clinical potential is limited by their moderate ability to survive after transplantation. To overcome these limitations, their encapsulation within protective environment would be beneficial. In this study, tunable calcium-alginate hydrogels obtained through molding method using external or internal gelation were investigated as a new strategy for hMuStem cell encapsulation. The mechanical properties of these hydrogels were characterized in their fully hydrated state by compression experiments using Atomic Force Microscopy. Measured elastic moduli strongly depended on the gelation mode and calcium/alginate concentrations. Values ranged from 1 to 12.5 kPa and 3.9 to 25 kPa were obtained for hydrogels prepared following internal and external gelation, respectively. Also, differences in mechanical properties of hydrogels resulted from their internal organization, with an isotropic structure for internal gelation, while external mode led to anisotropic one. It was further shown that viability, morphological and myogenic differentiation characteristics of hMuStem cells incorporated within alginate hydrogels were preserved after their release. These results highlight that hMuStem cells encapsulated in calcium-alginate hydrogels maintain their functionality, thus allowing to develop muscle regeneration protocols to improve their therapeutic efficacy.

1. Introduction

The identification in several tissues of adult stem cells (ASC) with demonstrated myogenic potential has paved the way for new therapeutic proposals in the field of regenerative medicine for muscle diseases [1–3]. The specific proliferation and differentiation properties of myoblasts were initially exploited for use in cell-based therapeutic strategies for muscular dystrophy. Myoblasts are the natural myogenic descendants of muscle-resident stem cells called satellite cells, and are responsible for ensuring post-natal growth and tissue repair [4]. However, myoblasts showed poor efficacy following administration into severely affected muscle, mainly due to an inability to successfully survive and integrate into host tissue [5]. These findings spurred further investigation aimed at identifying other cell candidates with better engraftment capacity in dystrophic muscle.

MuStem cells, a type of ASC identified in muscle tissue from healthy dogs and humans, have been extensively studied for their muscle regeneration potential. *In vitro* studies using conventional two-dimensional (2D) cell culture systems showed that MuStem cells have a high capacity for proliferation and naturally commit to the myogenic lineage [6,7]. In terms of phenotype and plasticity, MuStem cells were identified as early myogenic-committed progenitors with a mesenchymal perivascular profile, and displayed oligopotency through their commitment into myocytes, osteocytes or adipocytes after incubation in specific cell induction media [7,8]. Their robust capacity to form new muscle fibers has been demonstrated *in vivo* using multiple transplantation protocols in various animal models of acute muscle injury, including Duchenne muscular dystrophy (DMD) and myocardial infarction [7,9–11]. In these different contexts, the repeated detection of hundreds of donor nuclei fused with host muscle fibers several weeks after MuStem cell administration indicated an ability to engraft and maintain myogenicity. Overall, these preclinical findings support

* Corresponding author.
E-mail address: melanie.marquis@inrae.fr (M. Marquis).

https://doi.org/10.1016/j.ijbiomac.2024.130823
Received 8 January 2024; Received in revised form 20 February 2024; Accepted 11 March 2024
Available online 15 March 2024

MuStem cells as an attractive candidate for regenerative medicine in muscle diseases. Nonetheless, their overall therapeutic potential remains somewhat restricted by their moderate ability to survive and integrate into the host tissue despite clear superiority with respect to myoblasts and other ASC types [12].

In recent years, several studies have shown that the microenvironment in which cells evolve *in vitro* has a strong impact on their behavior, including proliferation, migration and differentiation [13–16]. Indeed, cells transform external stimuli received from their direct physical microenvironment into biochemical signals, resulting in the activation of specific genetic programs that control differentiation and proliferation of cells [17]. One of the most widely described cell signaling pathway involves the transcriptional coactivators YAP (yes-associated protein) and TAZ (PDZ-binding motif), which are known to mediate organ growth [18,19]. Engler et al. described the lineage commitment of cells as a function of their capacity for tissue mimicry, and showed that the mechanical characteristics of the surrounding extracellular matrix (ECM), such as elastic modulus, are key parameters that strongly influence cellular activities [20]. This suggests that strict control of the microenvironment in the *in vitro* conditioning and transplantation stages is essential to accurately optimize the overall therapeutic impact. To open up new transplantation strategies with MuStem cells transplantation, a better understanding of their behavior in the physical microenvironment is required to enhance their survival capacities and integration into the host tissue during the delivery protocol.

Emergence of three dimensional (3D) biological model systems provides a unique opportunity for the study of human biology and disease modeling. Tissue biomimicry approaches using biomaterials based on hydrogel networks with mechanical properties closely resembling those of the targeted tissue have been developed [21–23]. Hydrogels have a strong affinity for water, resulting in a highly hydrophilic network that closely matches that of the natural ECM. Multiple parameters, including the chemical composition of hydrogel components, the cross-linking density of the network, and its mechanical properties must be considered to create the most favorable environment to maintain cell activities. There are two main types of hydrogels, each of which differs in terms of network stability [24,25]. Chemical hydrogels are irreversible and are formed by specific functional groups of polymer chains linked by covalent bonds. By contrast, physical hydrogels are reversible, since their networks are maintained by non-covalent interactions induced by temperature, pH, or ionic strength changes. Alginate, a polysaccharide extracted from brown algae, is one of the natural polymers most commonly used in tissue engineering owing to its biocompatibility, low toxicity, and ability to form a hydrogel network [26–29]. In the presence of divalent cations such as calcium (Ca), alginate forms physical hydrogels based on Ca-mediated chain-chain associations following the egg-box model [30]. This type of hydrogel is particularly interesting given its natural origin and its properties of reversibility and degradability [28]. Moreover, with a wide range of elastic moduli (3–500 kPa) depending on reaction conditions, alginate hydrogels possess mechanical properties resembling those of biological tissues, making them suitable for biomimicry approaches [31–33]. For instance, previous studies of muscle tissues reported elastic moduli of 12 kPa in skeletal (*tibialis anterior* [TA]) muscle [34] and 21 kPa in cardiac muscle (left ventricle) [35]. Importantly, the mechanical properties of alginate hydrogels can be tuned to better match the targeted tissue by adjusting their physicochemical parameters, including gelation mode, alginate molecular weight, alginate and divalent cation concentrations, as well as blending and grafting with other polymers [36–41].

The main objective of this study was to develop physical alginate- and Ca-based hydrogels with the aim of preserving viability and myogenic potential of encapsulated human MuStem (hMuStem) cells. This point is crucial for their further therapeutic use. Firstly, the impact of alginate and Ca concentrations on the mechanical properties of hydrogels, prepared using two distinct gelation modes, external gelation (EG) or internal gelation (IG), was evaluated. For this purpose, several Ca-alginate hydrogels were generated using an experimental central composite design and their elastic moduli were systematically determined in their fully hydrated state at the cell level by Atomic Force Microscopy (AFM). Next, the diffusion of two fluorescein isothiocyanate (FITC)-labeled dextran derivatives was assessed to determine whether the hydrogel structure, evaluated using scanning electron microscopy (SEM), enabled the diffusion of small molecules secreted by the cells and nutrients essential for cell survival. Finally, the impact of the mechanical characteristics of these 3D artificial matrices on viability, morphology, and myogenic differentiation of encapsulated hMuStem cells was evaluated.

2. Materials and methods

2.1. Chemicals

Sodium alginate powder (Protanal TM LF10/60FT, M_w 180,000 g/mol, Mannuronate/Guluronate ratio of 0.4) was obtained from FMC Biopolymer (USA). The alginate powder was sterilized by steam autoclave (121 °C, 20 min), which resulted in a decrease in alginate molecular weight. The M_w of 85,000 g/mol of alginate derivative was determined by high-performance size-exclusion chromatography (HPSEC, Proinence Schimadzu, Japan) coupled with multiangle light scattering (MALS, Dawn Heleos-II, Wyatt Technology, CA, USA) [42]. Freeze-dried calcium carbonate ($CaCO_3$) powder (5 μm diameter particles) was provided by Mikhart Provençal S.A. Olive oil, calcium chloride ($CaCl_2$) powder and acetic acid were purchased from Sigma-Aldrich (MO, USA). Ultra-Pure™ Agarose was purchased from Invitrogen (Paisley, UK).

2.2. Preparation of solutions

Alginate (0.3, 0.6, 2.0, 4.0, 3.7 and 7.4 wt%) was dissolved either in ultra-pure water or culture medium for 2 h. $CaCO_3$ powder (5 μm diameter particles) was dispersed either in ultra-pure water or culture medium at 0.5 wt%. $CaCl_2$ solution (30, 100 and 170 mmol/L) was prepared in either ultra-pure water or culture medium. Acetic acid was solubilized in olive oil at 0.25 wt%. Agarose (5 % w/v) was dissolved in ultra-pure water at 100 °C under stirring, supplemented with $CaCl_2$ and poured into multi-well plate.

2.3. Preparation of hydrogels by molding methods

2.3.1. External gelation (EG)

EG was carried out by diffusion of a solubilized cross-linker, Ca, from the bottom of an underlying $CaCl_2$-loaded agarose layer to the top of the alginate solution. For this purpose, 1 mL or 300 μL of $CaCl_2$-loaded agarose (30, 100 or 170 mmol/L) were respectively poured into a 12-well (for AFM and SEM experiments) or 48-well (for diffusion experiments) plate. Next, 1 mL or 150 μL aqueous alginate solution (0.3, 2.0 or 3.7 wt%), respectively, was poured on top of the agarose layer. After 2 h of incubation at room temperature (RT), hydrogels were unmolded by direct addition of the corresponding aqueous $CaCl_2$ solution (30, 100 or 170 mmol/L) to each well. Hydrogels were then incubated in corresponding $CaCl_2$ solutions for at least 1 h to equilibrate the Ca concentration (Table S1).

2.3.2. Internal gelation (IG)

IG was induced by decreasing the pH inside the alginate solution containing $CaCO_3$ particles as the cross-linking agent in an inactive form placed at the bottom of the well. Acetic acid, used as a solubilization agent, diffuses from the top oil phase to the bottom alginate phase and triggers the release of Ca^{2+} ions, resulting in the formation of a hydrogel. Alginate (0.6, 4.0 or 7.4 wt%) and $CaCO_3$ (0.5 wt%) aqueous solutions were mixed (1:1, v/v) and 1 mL or 300 μL of the resulting solution, respectively, poured into a 12-well (for AFM and SEM experiments) or

48-well (for diffusion experiments) plate. Next, 2 mL or 600 μL of olive oil supplemented with acetic acid (0.25 wt%) was poured onto the aqueous alginate/$CaCO_3$ phase. After 2 h of incubation at RT, hydrogels were unmolded after replacement of the oil phase with the corresponding aqueous $CaCl_2$ solution (30, 100, or 170 mmol/L). Hydrogels were then incubated in corresponding $CaCl_2$ solutions for at least 1 h to equilibrate the Ca concentration (Table S1).

2.4. Preparation of calcium-alginate hydrogel following an experimental design

To evaluate the impact of Ca and alginate concentrations on the structural and mechanical properties of the hydrogels prepared using EG and IG methods, a 2^2 central composite design was constructed with 2-level variables coded (−1, +1) (Table 1). Level 0 was represented by central points (CP), performed in triplicate. Quadratic effects were determined by 4 "star" points (SP). Analysis of variance (ANOVA), regression analysis, and graphical study were conducted using StatGraphics 18.

2.5. Atomic force microscopy experiments

Mechanical properties of alginate hydrogels (n = 3, independent preparation) were assessed using a NanoWizard® atomic force microscope (AFM, JPK Instruments, Germany) operating in $CaCl_2$ aqueous solutions at RT (20 °C). Cantilevers (SQube) with a colloidal glass sphere of 5 μm in diameter were used to perform indentation experiments by measuring force-distance curves. The spring constant was calibrated using the thermal noise method implemented in the AFM setting (JPK software), with values of 0.12–0.18 $N{\cdot}m^{-1}$. Prior to indentation measurements, cantilever sensitivity was systematically measured from the slope of force-distance curves performed on glass. For each hydrogel of approximately 4-mm thickness, approach-retract force-distance curves were firstly performed to determine the maximum force to be applied corresponding to a maximum indentation depth of ~500 nm. Next, 10–20 force-distance curves were recorded at different locations for each hydrogel at a constant speed of 1 μm/s. This low speed was used to neglect the hydrodynamic drag forces exerted on the cantilever by the liquid medium [43]. These raw curves were then converted into force-indentation (F-δ) curves and the approach part was fitted using the Hertz model to determine the apparent elastic modulus of the hydrogels [44,45] using the following Eq. (1):

$$F = \frac{4}{3}\sqrt{R_{tip}}\,\frac{E_H}{1-\nu_H^2}\,\delta^{3/2} \quad (1)$$

where R_{tip} is the AFM tip radius, and E_H and ν_H are the elastic modulus and the Poisson's ratio of the hydrogel, respectively. In these experiments, the following parameters were used: R_{tip} = 2.5 μm and ν_H = 0.5 (the widely accepted value for hydrogels) [45].

Table 1
Experimental design parameters for independent variables used for EG and IG gelation processes. SP, star point, CP, central point. Matrix of the 2^2 central composite design.

Variable/ n°. of variables	Alginate concentration (wt %)	$CaCl_2$ concentration (mM)
−1 − 1	0.3	30
−1 + 1	0.3	170
+1 + 1	3.7	170
+1–1	3.7	30
SP1	2	170
SP2	2	30
SP3	0.3	100
SP4	3.7	100
CP1	2	100
CP2	2	100
CP3	2	100

2.6. Analysis of hydrogel structure by scanning electron microscopy

Ca-alginate hydrogel structures were examined with an environmental scanning electron microscope (ESEM, FEI Quanta 200 FEG, Netherlands). SEM images were obtained under low vacuum using frozen (−80 °C) and freeze-dried samples.

2.7. Diffusion properties of hydrogels

The diffusion properties of the hydrogels were studied by adapting a previously described protocol [46,47]. Briefly, hydrogels (n = 2, independent preparation) were placed at the bottom of chambered coverslips (Ibidi, Germany) and incubated for 24 h at RT in ultra-pure water containing 1 mg/mL of FITC-dextran at 2 different molecular weights: 20 kDa and 2000 kDa. Fluorescence intensity was measured by confocal laser scanning microscopy (CLSM; Nikon Eclipse N-Storm C2Si, Europe). FITC emission fluorescence was recorded between 515 and 555 nm after excitation at 488 nm in order to quantify the amount of dextran diffused inside hydrogels. Images were analyzed with ImageJ software (version 2.1.0/1.53c, https://imagej.nih.gov) to determine fluorescence intensities inside and outside the hydrogels and inside/outside (I/O) ratio was calculated. A ratio of 1 indicates a total homogenization of FITC-dextran molecules inside and outside the hydrogels. Results were expressed as the I/O ratio over time. Diffusion experiments were performed in duplicate for each condition and each time-point.

2.8. Biological activity of calcium-alginate hydrogel-encapsulated human MuStem cells

2.8.1. Cell culture conditions

Human MuStem cells were isolated from *paravertebralis* muscle biopsies from patients free of known muscle disease and who had undergone surgery for acute scoliosis at the Department of Pediatric surgery of the Centre Hospitalier Universitaire (CHU) de Nantes (France). Human MuStem cells were obtained from patients who had given written consent. All protocols were approved by the Clinical Research Department of the CHU (Nantes, France), according to the rules of the French Regulatory Health Authorities (Approval Number: MESR/DC-2010-1199). A biological sample bank was created in compliance with national guidelines regarding the use of human tissue for research (Approval Number: CPP/29/10). Human MuStem cells were isolated and characterized as previously established [6,8]. Cells were expanded in complete culture medium (DMEM, DMEM 4.5 g/L glucose and M199 mix [Fischer Scientific, France]) supplemented with 10 % fetal calf serum (Sigma-Aldrich), 1 % PSF mix (10,000 IU/mL penicillin, 10 mg/mL streptomycin 25 μg/mL fungizone; Sigma-Aldrich, France), 5 % horse serum (Sigma, France), 0.5 % chicken embryo extract (Clinisciences, France), 10 ng/mL human recombinant leukemia inhibitory factor (Sigma, France), 10 ng/mL human recombinant basic fibroblast growth factor (bFGF; Stemcell Technologies, France), 25 ng/mL human recombinant epidermal growth factor (EGF; Stemcell Technologies, France), and 25 ng/mL human recombinant stem cell factor (SCF; Cellgenix, Germany) under standard conditions at 37 °C in 5 % CO_2 and humidified atmosphere, and maintained at roughly 75 % confluence to avoid spontaneous myogenic differentiation. Cells were seeded on CELLstart substrate-coated plastic flasks (Invitrogen, France) and culture medium was replaced every 2 days. For this study, cells underwent *in vitro* expansion corresponding to 12 to 16 cumulated population doublings.

2.8.2. Encapsulation of human MuStem cells in calcium-alginate hydrogels

Human MuStem cells were encapsulated inside Ca-alginate hydrogels prepared following the steps described in part 2.2. Experiments were performed using hydrogels with an elastic modulus of 12 kPa for EG and IG modes. For EG, 300 μL of 170 mmol/L $CaCl_2$-loaded agarose

was poured into a 48-well plate. Next, 150 μL of 2 wt% alginate solution, prepared in culture medium and containing 7×10^5 hMuStem cells, were poured on the top of the agarose layer. After 2 h of incubation in standard culture conditions hydrogels were unmolded with culture medium supplemented with 170 mmol/L $CaCl_2$ added directly to the wells and incubated 1 h to reach Ca equilibrium. For IG, 7.4 wt% alginate solution containing 7×10^5 hMuStem cells and 0.5 wt% $CaCO_3$ solution, both prepared in culture medium, were mixed (1:1, v/v) and 150 μL of the resulting solution poured into a 48-well plate. Next, 300 μL of olive oil supplemented with 0.25 wt% acetic acid was poured onto the aqueous alginate/$CaCO_3$ phase. After 2 h of incubation in standard culture conditions, hydrogels were unmolded after replacement of the oil phase by culture medium supplemented with 170 mmol/L $CaCl_2$ and incubated 1 h to reach Ca equilibrium. Finally, hydrogels were transferred into a 24-well plate and incubated with 2 mL of culture medium in culture conditions for further analysis.

2.8.3. Cell viability

Human MuStem cells encapsulated in Ca-alginate hydrogels with an elastic modulus of 12 kPa were cultured in proliferation medium for up to 8 days, and medium changed every 2 days. Cell viability was determined at days 1, 2 and 8 using classical trypan blue staining. To this end, encapsulated cells were released by degrading Ca-alginate hydrogels with 55 mmol/L sodium citrate, used as calcium chelating agent (10 min, 37 °C), followed by centrifugation (400 ×*g*, 10 min) and staining with trypan blue (VWR, France). Cells were counted with hemacytometer. In parallel, viability assays were performed on cells encapsulated for 1 and 2 days using Live/Dead staining protocol. Briefly, Ca-alginate hydrogels containing cells were incubated in chambered coverslips (Ibidi, Germany) for 45 min in Live/Dead solution composed of 2 nuclear fluorochromes: 5.00 μg/mL Hoechst 33342 and 8.56 μg/mL Ethidium homodimer-1 (EthD-1), which stain the nuclei of viable and dead cells, respectively. Indeed, EthD-1 is known to quench Hoechst 33342 fluorescence on dead cells, when used at 6.2 μg/mL [48]. The labeled nuclei of hMuStem cells were directly imaged in chambered coverslips by CLSM (Zeiss LSM 780, Germany). For each acquisition, cell counting was performed by analyzing a stack of at least 10 images of a 10 μm-thick section using ImageJ Software (win64). Viability experiments with trypan blue staining and Live/Dead staining protocol were performed in triplicate for each EG and IG hydrogel from independent experiments ($n = 2$ for trypan blue staining, $n = 1$ for Live/Dead staining). In all cases, cell viability was calculated using the following Eq. (2):

$$Cell\ viability\ (\%) = \left(\frac{N_{live}}{N_{tot}}\right) \bullet 100\% \quad (2)$$

where N_{live} is the number of living cells and N_{tot} is the total cell number.

2.8.4. Proliferation and myogenic differentiation of human MuStem cells

Human MuStem cells encapsulated for 1 and 2 days were released by degrading Ca-alginate hydrogels with 55 mmol/L sodium citrate (10 min, 37 °C), followed by centrifugation (400*g*, 10 min). Cell suspension (700 μL) at a density of 2.4×10^4 cells/mL was seeded in a 24-well plate with proliferation medium. During the first 5 days of culture, the medium was changed every 2 days. Cell proliferation was evaluated up to day 5 by phase contrast microscopy acquisitions in 3 replicate wells. After 5 days under proliferative conditions, commitment towards myogenic differentiation was induced by progressive depletion of the nutrient load (cessation of medium renewal). Differentiation ability was assessed at day 21 by phase contrast microscopy based on the formation of multinucleated cells (myotubes) expressing the sarcomeric myosin heavy chain isoform (sMHC). Cultures were fixed in 4 % paraformaldehyde, treated with 0.5 % Triton X-100/20 % (w/v) goat serum in PBS, and incubated (1 h, 37 °C) with anti-human MF20 Ab (1:200, Developmental Studies Hybridoma Bank [DSHB], IA, USA). Specific Ab binding was revealed using biotinylated secondary goat-anti-mouse Ab (1:300, Dako). Ability of hMuStem cells to commit to differentiation was determined by the presence of nuclei within $MF20^+$ myotubes (>2 nuclei) in 3 replicate wells.

2.9. Statistical analysis

All experimental results were expressed as mean values ± SD (Standard Deviation). Cell viability data were analyzed by Student's *t*-test to determine statistical differences between different hydrogel gelation preparations and cell staining conditions using GraphPad Prism software, v6.0f (GraphPad Software, La Jolla, CA, USA). Diffusion properties were analyzed in R software, v4.2.3, by one-way analysis of variance (ANOVA) and Tukey's multiple comparison tests to determine statistical differences between different hydrogel structures. Levels of significance were set at $^*p < 0.05$ and $^{**}p < 0.01$.

3. Results and discussion

3.1. Impact of gelation mode on elastic modulus of calcium-alginate hydrogels

The first objective of the present study was to evaluate the influence of the two distinct gelation modes used to generate cylindrical Ca-alginate hydrogels, of 21 mm in diameter and 4 mm in height, on the mechanical and structural properties of the resulting networks. Hydrogels were prepared using molding methods in multi-well plates (Fig. 1), using two distinct gelation processes that differ in terms of the Ca source and its diffusion inside the network. The EG mode involves induction of gelation by diffusion of solubilized Ca ions from the bottom of a $CaCl_2$-loaded underlying agarose layer to the top of the alginate solution (Fig. 1A) [49]. By contrast, the IG mode involves gelation by solubilization of Ca ions from $CaCO_3$ particles dispersed inside the alginate solution through a pH decrease mediated by acetic acid diffusion from the upper oil layer (Fig. 1B) [50]. These gelation modes were previously used for cell encapsulation in other studies. Swioklo et al. demonstrated maintenance of human adipose-derived stem cell functionality following encapsulation into Ca-alginate discs using EG [51]. Akbari et al. developed a microfluidic method to encapsulate mouse breast cancer cells by IG, and showed that encapsulated cells also retained their biological activities [52]. However, to our knowledge, no comparative study assessed the impact of gelation mode on the mechanical and structural properties of Ca-alginate hydrogels and on the viability and biological activities of cells encapsulated within these hydrogels. For this purpose, a 2^2 central composite design was applied for EG and IG modes to assess the effect of 2 variables, alginate and Ca concentrations, on the elastic modulus of the resulting hydrogels (Table 1). The experimental domain was delimited by the solubilization capacity of alginate and Ca, the viscosity of alginate solutions, and the effective gelation. To ensure Ca equilibrium inside the hydrogels at the end of the process, each hydrogel was incubated after unmolding in corresponding $CaCl_2$ aqueous solution. Conditions of incubation chosen (Table S1) were based on previous studies describing the mechanism that occurs during external gelation of alginate induced by Ca cations [54,55]. Thus, it can be assumed that a complete gelation was reached at the end of the process with a Ca concentration at equilibrium for both gelation modes.

The mechanical properties of various Ca-alginate hydrogels obtained by both EG and IG were systematically measured by AFM in fully hydrated conditions, *i.e.*, in $CaCl_2$ aqueous solution used for storage (Fig. 2A). Indentation experiments were performed by recording approach-retraction force-distance curves in different locations for each hydrogel. Two force-indentation curves measured in EG and IG hydrogels prepared with 2 % alginate and 170 mM Ca concentrations were shown in Fig. 2B. Hysteresis between the approach and retraction parts of the curves was observed, indicating the time-dependent nature of the hydrogels' mechanical properties. Recently, it was shown that relaxation

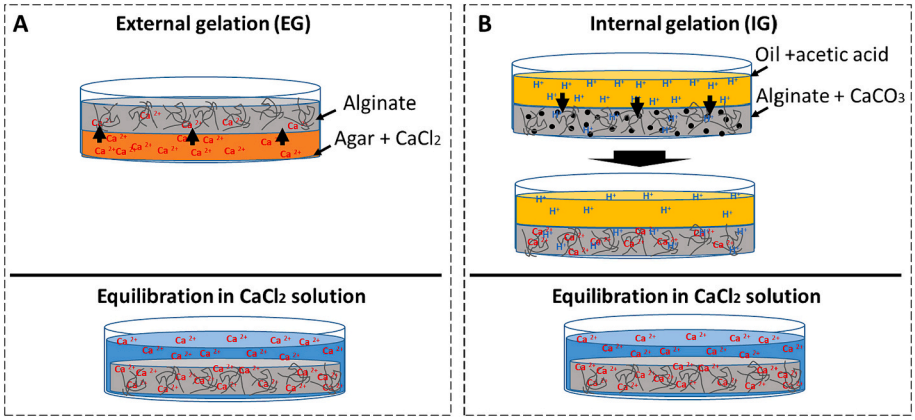

Fig. 1. Molding process and hydrogel formation using (A) external and (B) internal gelation modes.

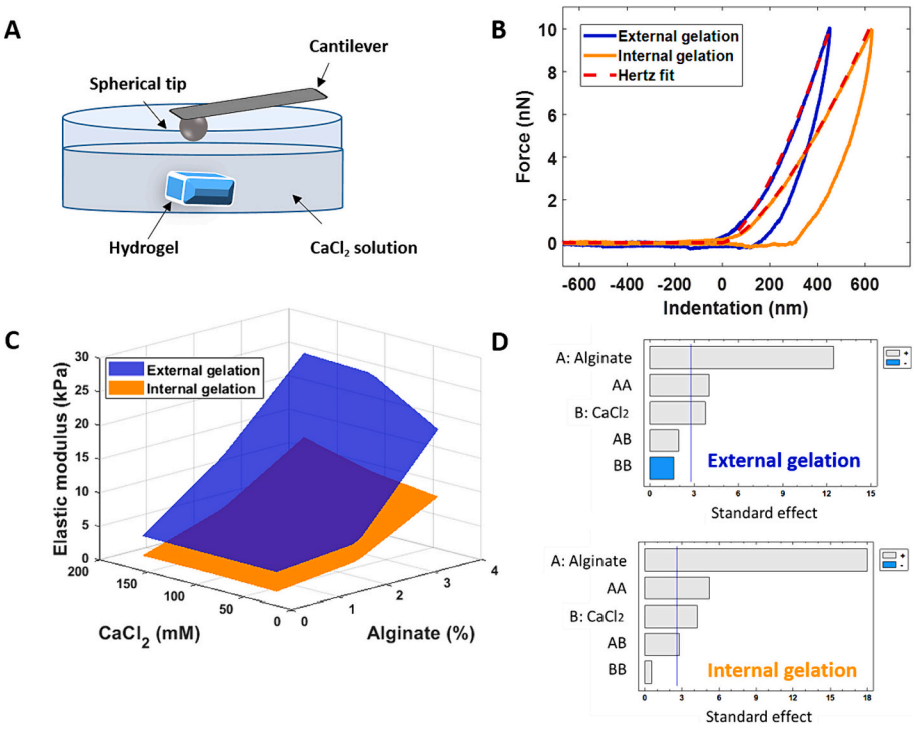

Fig. 2. (A) Schematic representation of AFM indentation experiments performed on hydrogel in liquid medium. (B) Experimental force-indentation curves measured in hydrogels generated using external and internal gelation modes with 2 % alginate and 170 mM *Ca*. Fitting of the approach curve using the Hertz model to determine the elastic modulus of hydrogels. (C) Response surface of the elastic modulus of hydrogels as a function of alginate and Ca concentrations for external and internal gelation modes. (D) Pareto charts depicting the influence of 2 variables (alginate and Ca concentrations) and their interactions on the elastic moduli for external and internal gelation modes.

processes in polysaccharide hydrogels crosslinked with Ca arise from viscoelastic effects [43]. Here, only the elastic component was evaluated. Relaxation times associated with these dissipative processes were not investigated. The Hertz model was then applied to fit the approach part of the force-indentation curves, allowing to extract the apparent elastic modulus [44,45]. As shown in Fig. 2B, good agreement between fitted and experimental approach curves for 2 EG and IG hydrogels was observed. Elastic modulus values for EG and IG hydrogels were 13.1 kPa and 5.8 kPa, respectively. The elastic moduli determined for hydrogels generated using both gelation modes at different alginate and Ca concentrations were presented in Table S2. Elastic moduli ranged from 1 to 12.5 kPa and 3.9 to 25 kPa for IG and EG hydrogels, respectively. The lowest elastic modulus (1 kPa) was obtained for IG hydrogels formulated using 0.3 wt% alginate and 30 mM Ca, while the highest elastic modulus (25 kPa) was obtained for EG hydrogels prepared with 3.7 wt% alginate and 170 mM *Ca*. EG hydrogels exhibited higher elastic moduli than IG hydrogels generated with the same alginate and Ca concentrations (Fig. 2C). The response surface of elastic modulus revealed that for both gelation modes mechanical properties markedly increased with alginate and Ca concentrations (see Supporting Information, *Statistical analysis* for response surface equations and validation of models; Tables S3 and S4). Pareto charts revealed the impact of the alginate and Ca concentrations (acting as 2 variables) and their interactions on the elastic modulus measured in hydrogels generated using the 2 gelation modes (Fig. 2D). The most significant positive effect on elastic modulus response came from alginate concentration in comparison to that of *Ca*. Increases in alginate concentration had a more pronounced effect on elastic modulus than increases in Ca concentration. This effect was observed for both gelation modes, although the studied variables and their interactions had more pronounced effects in IG *versus* EG

hydrogels.

The obtained results indicated a strong influence of gelation mode on the mechanical properties of hydrogels. The elastic modulus values obtained were comparable with those reported for alginate microgels with values of 0.3–16 kPa, depending on alginate molecular weight and calcium concentration [53]. Elastic moduli of ~9 kPa and ~17 kPa were reported for macroscopic alginate hydrogels crosslinked with Ca following rheological measurements [54]. In another study, elastic moduli of 0.8–8 kPa were measured by AFM on Ca-infernan microgels [45]. In these different studies the elastic modulus of hydrogels also increased with polysaccharide and Ca concentrations. Interestingly, of the hydrogels developed for the present study, two possessed mechanical properties comparable to those of skeletal muscle (~12 kPa). They were obtained using both gelation modes: one using EG with 2.0 wt% alginate and 170 mM Ca, and the other using IG with 3.7 wt% alginate and 170 mM *Ca*. These two hydrogels that mimic muscle tissue were selected for a comparative *in vitro* study of the impact of the two gelation modes on the biological activities of hMuStem cells.

3.2. Structure of calcium-alginate hydrogels

Because the elastic moduli of hydrogels evolved differently depending on gelation mode, the internal structure of EG and IG hydrogels with three distinct elastic moduli (5, 12, and 25 kPa and 1, 5, and 12 kPa, respectively; Table S2) was analyzed. Internal organization based on a honeycomb-like structure was observed, in line with other studies on hydrogels [32,58]. Nevertheless, lamellar pores were observed in EG hydrogels, while IG hydrogels exhibited more spherical pores, indicating that EG and IG modes led to anisotropic and isotropic organization, respectively (Fig. 3). The anisotropic organization with lamellar structures observed in EG hydrogels most likely resulted from Ca diffusion across a gradient formed between the Ca-rich agarose layer and the Ca-free alginate solution, resulting in alginate chain associations perpendicular to Ca flow (Fig. 3A). This type of structural organization was already reported for divalent cations/polyuronate hydrogels, including alginate hydrogels [55–57]. In those studies, polysaccharide gelation resulted from the gradient of crosslinking cation concentration. The formation of rod-shaped fibrils composed of alginate chains oriented perpendicular to the cation flow, leading to the anisotropic structural organization of the gel was shown by small angle X-ray scattering [55]. Similarly, in another study, after association of polysaccharide chains by Ca, free chains were shown to diffuse in the opposite direction to the free cation diffusion, leading to the organization by "layers" [56]. In IG mode, insoluble $CaCO_3$ particles homogeneously distributed within alginate solution constituted the source of crosslinking Ca ions. Their slow dissolution, induced by a decrease in pH by acid diffusion from the upper oil layer, provided soluble Ca, which induced the cross-linking of surrounding alginate chains, thus leading to the formation of isotropic structures (Fig. 3B). Such isotropic organization has already been reported in other studies based on $CaCO_3$-alginate hydrogels [36,50,58].

In general, the AFM tip-hydrogel surface contact can be modelled by two springs (normal and lateral) having the same spring constant in the case of an isotropic structure, while these constants are different in anisotropic structure. Mechanical properties measured by AFM are in accordance with the internal structure of hydrogels observed in Fig. 3. Indeed, during AFM force-indentation experiments, the lamellar anisotropic structure stressed in bending showed greater lateral contact stiffness than the isotropic structure. Thus, under the same experimental conditions (alginate and Ca concentrations), the contact stiffness between the AFM tip and EG hydrogel will be higher than that measured for IG hydrogels. Higher elastic moduli measured for anisotropic hydrogels generated by EG, compared to those generated by IG, are most likely due to higher density of junction zones formed when soluble Ca diffuses freely within alginate solution and initiates alginate gelation following "egg box model". Such gelation mechanism leads naturally to thick junction zones organized in "layers". In the case of IG hydrogels, dissolution of Ca from $CaCO_3$ particles homogeneously dispersed within alginate solution may limit the number of thick junction zones, leading to hydrogel with lower cross-linking density.

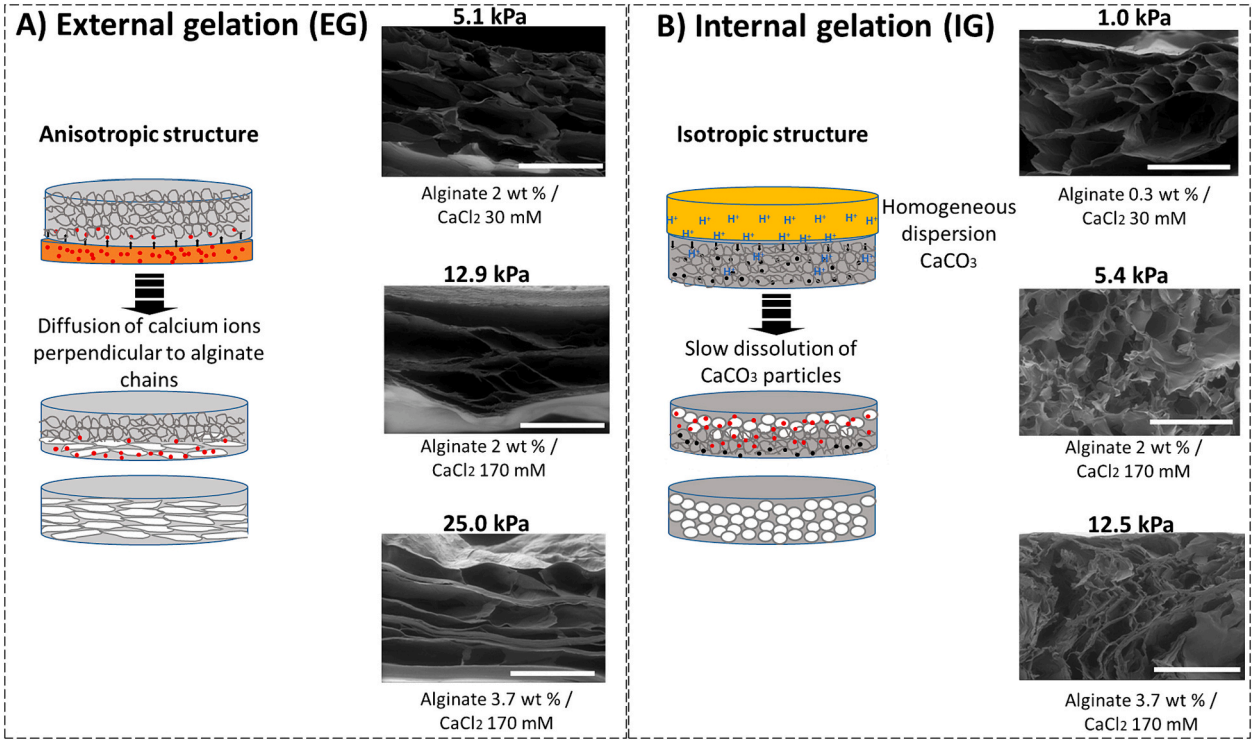

Fig. 3. Impact of gelation mode on physical parameters. Schematic structural organizations during the gelation processes. (A) External gelation leading to anisotropic organization with lamellar pores. (B) Internal gelation resulting in isotropic organization with spherical pores. Scale bar: 400 μm.

3.3. Diffusion properties of hydrogels

Next, the diffusion properties of Ca-alginate hydrogels generated by EG and IG were evaluated to determine whether pore shape and size can impact solute accessibility and diffusion rates. This information is important as the quality of the exchanges that occur within hydrogels will condition the extent to which cells encapsulated within these hydrogels can interact with their external environment in the context of *in vitro* expansion or transplantation for tissue remodeling. Indeed, soluble factors secreted by cells and/or host tissue as well as growth factors and other nutrients need to circulate freely through the hydrogel structure to ensure appropriate cell responses. To this end, two FITC-dextrans of different molecular weights were used. The hydrodynamic radius (Rh) of both macromolecules was determined using the following Eq. (3), as previously described [47]:

$$M_w = (1.4782 \cdot R_h)^{1.8136} \quad (3)$$

where M_w is the molecular weight (kDa) and R_h is the hydrodynamic radius (nm).

The hydrodynamic radii of low-molecular weight (LMW) FITC-dextran (20 kDa) and high-molecular weight (HMW) FITC-dextran (2000 kDa) were 7.0 and 89.4 nm, respectively. Diffusion of both dextran fractions was followed using CLSM in 3 IG hydrogels of 1, 5.1 and 12.5 kPa and 3 EG hydrogels of 3.9, 12.9 and 25 kPa. Next ratios of fluorescence intensities inside (I) and outside (O) hydrogels were determined after 6 h and 24 h of incubation (Fig. 4A). An I/O ratio of 0 indicates the absence of molecular diffusion through the hydrogel, while a ratio >0 indicates that diffusion rate depends on the mesh size of the hydrogel. An I/O ratio of 0.4 was considered to correspond to free molecular diffusion inside hydrogels, as previously reported [46,47]. For LMW FITC-dextran, maximal diffusion for all hydrogels was measured during the first 6 h of incubation, and tended to decrease with increasing elastic modulus (Fig. 4B, left graph). In EG hydrogels, maximum I/O ratio values were 0.90, 0.85 and 0.80 for elastic moduli of 3.9, 12.9 and 25.0 kPa, respectively. The corresponding values for IG hydrogels were 0.90, 0.61 and 0.62 for elastic moduli of 1.0, 5.1 and 12.5 kPa, respectively. While these results suggested slightly lower diffusion in isotropic structures (IG) for elastic moduli of 5.1 and 12.5 kPa ($p < 0.05$), small molecules of ~7 nm could diffuse freely (I/O ratios >0.4) despite constraints imposed by the internal structure of the hydrogel.

For HMW FITC-dextran diffusion, maximum I/O ratio values reached those observed for LMW FITC-dextran (I/O ratio >0.4) for low elastic moduli (1.0 and 3.9 kPa) (Fig. 4B, right graph). For medium and high elastic moduli (from 5.1 to 25 kPa), diffusion was low and occurred mainly during the first 6 h, reaching low I/O ratio values of 0.27–0.37. These findings revealed a marked difference in diffusion profiles between hydrogels with low *versus* medium/high elastic moduli regardless of the gelation mode used ($p < 0.01$). For hydrogels with a similar elastic modulus close to 12 kPa, a slight increase in I/O ratio was observed for EG hydrogels. These results suggested effective diffusion of larger molecules ~90 nm at low elastic moduli, regardless of the internal structure (anisotropic or isotropic). However, diffusion through hydrogels with medium/high elastic moduli was significantly restricted. The I/O ratios obtained for six alginate hydrogels were concordant with those measured for alginate and Si-HPMC hydrogels with elastic moduli of 16 kPa and 0.22 kPa, respectively [46,47]. Overall, these results indicates that the two types of hydrogels studied are compatible with free diffusion of small molecules, suggesting that they allow the circulation of nutrients necessary for metabolism of encapsulated cells.

3.4. Behavior of human MuStem cells in hydrogels mimicking the elastic moduli of skeletal muscle

Next the impact of Ca-alginate hydrogels on the biological properties of hMuStem cells encapsulated within EG and IG hydrogels with an elastic modulus of 12 kPa (*i.e.*, close to that of skeletal muscle) was investigated [34]. After encapsulation, cells were uniformly retained within both types of hydrogels (Fig. S2).

3.4.1. Cell viability

To determine whether the encapsulation process negatively affects hMuStem cells in any way, cell viability was evaluated after 1, 2 and 8 days in hydrogels using classical staining with trypan blue of a mean number of 40,000 freshly released cells. Viability rates were 80 % ± 6 %, 88 % ± 4 %, and 83 % ± 5 % at 1, 2, and 8 days post-encapsulation in EG hydrogels (Fig. 5A). In IG hydrogels, the corresponding viability rates were 86 % ± 9 %, 93 % ± 1 %, and 95 % ± 3 %. These results showed

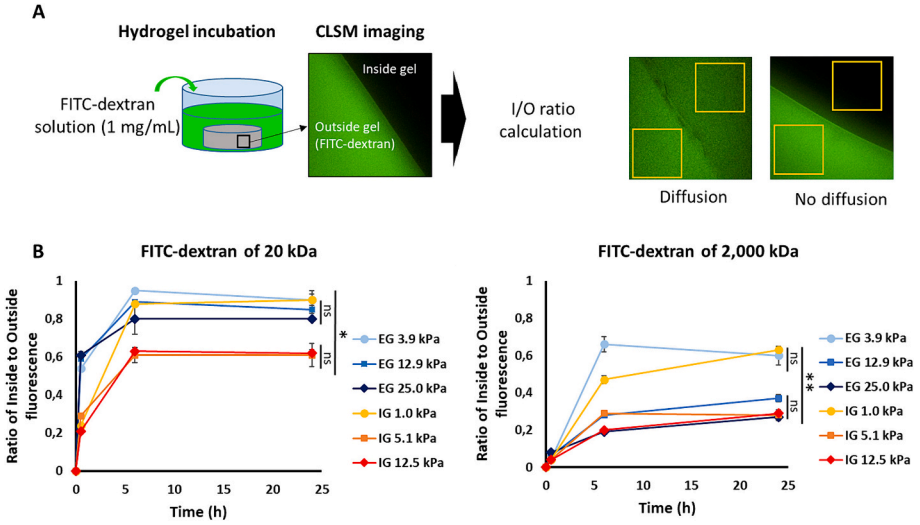

Fig. 4. (A) Methodology applied to monitor diffusion within hydrogels. Inside/outside (I/O) ratio was determined based on fluorescence intensities measured inside and outside hydrogels in square region of interest (ROI) of 200 μm × 200 μm in size. An I/O ratio of 1 indicates total homogenization of FITC-dextran molecules inside and outside the hydrogels. (B) Diffusion profiles determined 24 h after incubation with 20 kDa and 2000 kDa FITC-dextran. EG: light blue (•)/middle blue (■)/dark blue (◆); IG: yellow (•)/orange (■)/red (◆). Diffusion experiments were performed in duplicate for each condition and time-point. Data are expressed as the mean ± SD. Statistical analysis compared maximum I/O ratio values. Values of $p < 0.05$ were considered significant (*$p < 0.05$; **$p < 0.01$). ns, not significant. (For interpretation of the references to color in this figure legend, the reader is referred to the web version of this article.)

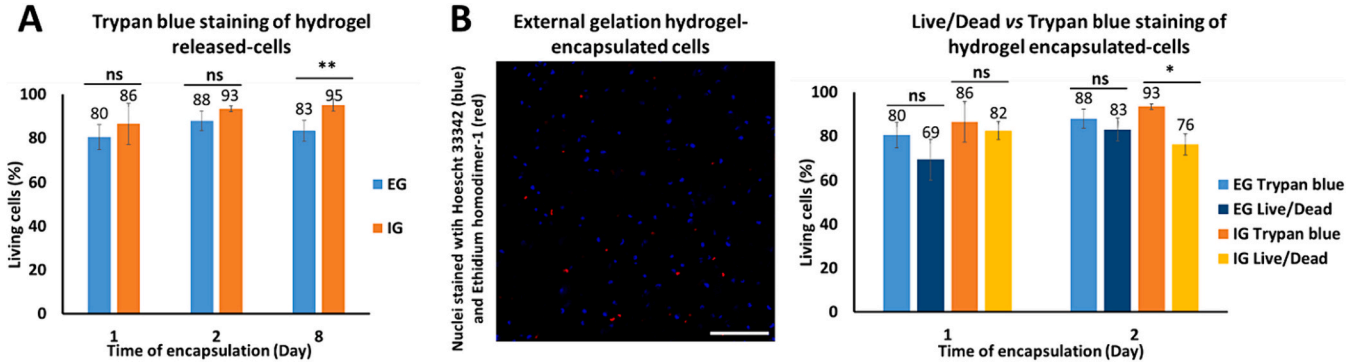

Fig. 5. Viability over time of hMuStem cells after encapsulation in 12 kPa Ca-alginate hydrogels. Determination of the yield of living cells per macrogel using. (A) Trypan blue staining. After dissolving hydrogels with sodium citrate, cells resuspended in culture medium were stained with trypan blue. Experiments ($n = 3$, independent encapsulation protocol) were performed in triplicate for both EG and IG hydrogels at each time-point (days 1, 2 and 8); (B) live/dead intracellular staining. Hydrogel-encapsulated cells were incubated at day 1 and 2 with 5 μg/mL Hoechst 33342 (blue) and 8.56 μg/mL EthD-1 (red) to stain nuclei of viable and dead cells, respectively. Typical CLSM images of cells encapsulated in hydrogels obtained at day 2. Scale bar, 160 μm. A single encapsulation experiment was performed in triplicate for both EG and IG hydrogels and at the 2 time-points (days 1 and 2). Comparison of cell viability values as determined by Live/Dead staining and trypan blue staining. Data are expressed as the mean ± SD. Values of $p < 0.05$ were considered significant ($^*p < 0.05$; $^{**}p < 0.01$). ns: not significant. (For interpretation of the references to color in this figure legend, the reader is referred to the web version of this article.)

that >80 % of hMuStem cells remained viable regardless of encapsulation time, gelation mode, and internal hydrogel structure. This indicated that hydrogels were compatible with *in vitro* maintenance of hMuStem cells. In addition, living cells inside Ca-alginate hydrogels were counted 1 and 2 days post-encapsulation using Hoechst 33342 and EthD-1 co-staining of a mean number of 70 cells (Fig. 5B). Proportions of living cells were 69 % ± 9 % and 83 % ± 5 % in EG hydrogels and 82 % ± 4 % and 76 % ± 5 % in IG hydrogels, respectively, in accordance with trypan blue staining, even though the proportion of live cells in IG hydrogels was slightly lower than that obtained with trypan blue staining of cells released from the hydrogels ($p = 0.03$). This may be due to the fact that some dead cells remained trapped in hydrogels and were therefore not counted in the trypan blue test. These viability rates were in accordance with those previously described for other cells encapsulated in alginate-based hydrogels [51,59,60]. Together, these results showed that the use of EG and IG hydrogels was compatible with the viability of encapsulated cells, suggesting potential as useful matrices for *in vitro* conditioning.

3.4.2. *Myogenic fate of hMuStem cells after encapsulation into calcium-alginate matrices*

The morphological features of hMuStem cells and their ability to commit to a myogenic differentiation pathway after encapsulation were studied to determine whether their encapsulation in a 3D Ca-alginate matrix would alter the biological properties of hMuStem cells. After 2 days of encapsulation in EG and IG hydrogels, hMuStem cells were released by dissolving the gels with sodium citrate, and seeded in standard 2D primary culture conditions ($n = 3$, independent experiments performed in triplicate). After 5 days, cells adhered to the matrix support and formed a culture composed of mainly thin, elongated spindle-shaped cells and small and refringent round cells, as usually observed in cultures of cells that were never encapsulated (Fig. 6, top line). This finding indicated the absence of any alteration in morphological characteristics following cell encapsulation. When primary cultures reached 80 % confluence, myogenic differentiation was induced ($n = 1$, independent experiment performed in triplicate). After 16 days, numerous cells that aligned and fused to form multinucleated cells were detected by the expression of sarcomeric myosin heavy chain isoform,

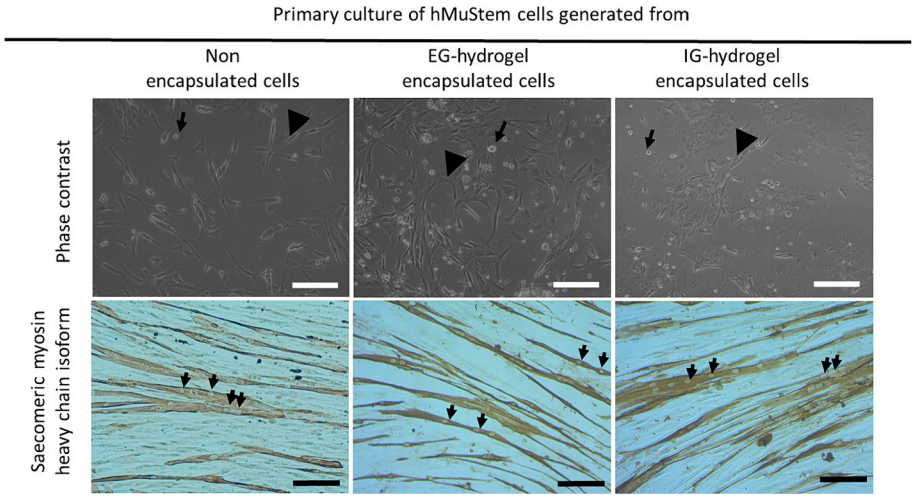

Fig. 6. Biological features of hMuStem cells in standard 2D culture conditions, with or without prior encapsulation for 2 days in EG or IG hydrogels. (Top line) Morphological examination by phase contrast after 5 days in growth medium revealing formation of a primary culture mainly composed of adherent, thin, spindle-shaped cells (arrowhead) and refringent round cells (arrow) in the 3 conditions tested. (Bottom line) Immunolabeling directed against the sarcomeric isoform of the myosin heavy chain showing the presence of myotubes (multinucleated cells; arrow) in the 3 conditions tested after 16 days in myogenic differentiation induction conditions. Scale bar: 200 μm and 100 μm in top and bottom line, respectively.

strongly resembling the behavior of non-encapsulated cells (Fig. 6, bottom line). These findings showed that the hMuStem cells, despite passage in EG or IG hydrogels, maintained their myogenic differentiation potential, as described previously in standard culture conditions [6]. These results were in line with previous studies performed using various types of cells encapsulated in alginate-based hydrogels. Li et al., reported that mouse preosteoblasts (MC3T3-E1) encapsulated in Ca-alginate-gelatin capsules retained their capacity for adhesion, spreading, and proliferation after release and re-inoculation. Moreover, upon osteogenic induction, these cells were able to differentiate [60]. Similarly, Leijs et al. demonstrated the multi-lineage differentiation capacity of mesenchymal stem cells (MSCs) released after encapsulation in alginate hydrogels [61]. Together, these findings showed that Ca-alginate hydrogels displaying similar elastic modulus (~12 kPa), but different internal organization resulting from two distinct gelation modes, allow for preservation of the morphological characteristics and myogenic differentiation of hMuStem cells.

4. Conclusion

In the present study, the impact of the gelation mode on the mechanical properties of Ca-alginate hydrogels and the biological characteristics of encapsulated hMuStem cells was investigated. This step remains crucial before incorporation the encapsulation of hMuStem cells as a suitable strategy for *in vivo* transplantation protocols. Two experimental variables, alginate and Ca concentrations, and two distinct gelation modes, external *versus* internal, were applied to produce a set of hydrogels with a large range of mechanical properties, measured in the fully hydrated state by AFM. It appeared that the conditions used for alginate gelation, in particular Ca distribution and availability, were key determinants of the mechanical properties and internal structure of the resulting hydrogels. Indeed, EG hydrogels exhibited elastic moduli between 3.9 and 25 kPa, while elastic moduli of IG hydrogels were considerably lower ranging from 1 to 12.5 kPa. For the same alginate and Ca concentrations, EG hydrogels displayed higher elastic moduli than IG hydrogels. The mechanical properties of these two types of hydrogels resulted from their different internal organizations, characterized by either anisotropic lamellar or isotropic spherical pore structure, observed for EG and IG hydrogels, respectively. Diffusion of LMW molecules inside EG and IG hydrogels was compatible with the diffusion of nutrients essential for the survival of hMuStem cells after encapsulation. *In vitro* analyses of hMuStem cells released from EG and IG hydrogels with elastic moduli similar to that of the skeletal muscle (~12 kPa) indicated that their encapsulation had no impact on cell viability, morphology and myogenic differentiation. Both gelation approaches can be applied for hMuStem cell encapsulation. Future studies will be needed to characterize the phenotypic profile and secretory activities of encapsulated hMuStem cells. This will provide a better understanding of the impact of artificial matrices on the biological properties of these promising candidates for regenerative medicine for muscle diseases.

Supporting information

Preparation of hydrogels by molding methods; Experimental design; Statistical analysis of experimental design responses and the validation of models; Additional data on cellular activities of hMuStem cells in skeletal mimetic hydrogels.

Author statement

We confirm that the manuscript has been read and approved by all named authors and that there are no other persons who satisfied the criteria for authorship but are not listed. We further confirm that the order of authors listed in the manuscript has been approved by all of us.

CRediT authorship contribution statement

Mélanie Marquis: Writing – review & editing, Writing – original draft, Methodology, Investigation, Formal analysis, Conceptualization. **Agata Zykwinska:** Writing – review & editing, Writing – original draft, Conceptualization. **Bruno Novales:** Investigation. **Isabelle Leroux:** Investigation. **Cindy Schleder:** Investigation. **Julien Pichon:** Methodology, Investigation. **Stéphane Cuenot:** Writing – review & editing, Writing – original draft, Methodology, Investigation, Formal analysis, Conceptualization. **Karl Rouger:** Writing – review & editing, Supervision.

Declaration of competing interest

The authors declare no competing financial interests.

Data availability

Data will be made available on request.

Acknowledgment

The authors wish to thank Florelle Desgenetez for her technical support in the experimental design and the generation of Ca-alginate hydrogels. Thanks also to Corinne Sinquin and Chantal Thorin for HPSEC-MALS analysis and statistical analysis, respectively. We thank Jean-Thomas Vilquin (UMRS 974, Paris, France) and Dominique Hourdet (SIMM; ESPCI, Paris, France) for helpful discussion.

Appendix A. Supplementary data

Supplementary data to this article can be found online at https://doi.org/10.1016/j.ijbiomac.2024.130823.

References

[1] D. Costamagna, E. Berardi, G. Ceccarelli, M. Sampaolesi, Adult stem cells and skeletal muscle regeneration, Curr. Gene Ther. 15 (2015) 348–363, https://doi.org/10.2174/1566523215666150630121024.
[2] S.-V. Forcales, Potential of adipose-derived stem cells in muscular regenerative therapies, Front. Aging Neurosci. 7 (2015), https://doi.org/10.3389/fnagi.2015.00123.
[3] E. Negroni, T. Gidaro, A. Bigot, G.S. Butler-Browne, V. Mouly, C. Trollet, Invited review: stem cells and muscle diseases: advances in cell therapy strategies, Neuropathol. Appl. Neurobiol. 41 (2015) 270–287, https://doi.org/10.1111/nan.12198.
[4] P. Seale, M.A. Rudnicki, A new look at the origin, function, and "stem-cell" status of muscle satellite cells, Dev. Biol. 218 (2000) 115–124, https://doi.org/10.1006/dbio.1999.9565.
[5] Y. Fan, M. Maley, M. Beilharz, M. Grounds, Rapid death of injected myoblasts in myoblast transfer therapy, Muscle Nerve 19 (1996) 853–860.
[6] J. Lorant, C. Saury, C. Schleder, F. Robriquet, B. Lieubeau, E. Négroni, I. Leroux, L. Chabrand, S. Viau, C. Babarit, M. Ledevin, L. Dubreil, A. Hamel, A. Magot, C. Thorin, L. Guevel, B. Delorme, Y. Péréon, G. Butler-Browne, V. Mouly, K. Rouger, Skeletal muscle regenerative potential of human MuStem cells following transplantation into injured mice muscle, Mol. Ther. 26 (2018) 618–633, https://doi.org/10.1016/j.ymthe.2017.10.013.
[7] K. Rouger, T. Larcher, L. Dubreil, J.Y. Deschamps, C. Le Guiner, G. Jouvion, B. Delorme, B. Lieubeau, M. Carlus, B. Fornasari, M. Theret, P. Orlando, M. Ledevin, C. Zuber, I. Leroux, S. Deleau, L. Guigand, I. Testault, E. Le Rumeur, M. Fiszman, Y. Chérel, Systemic delivery of allogenic muscle stem cells induces long-term muscle repair and clinical efficacy in duchenne muscular dystrophy dogs, Am. J. Pathol. 179 (2011) 2501–2518, https://doi.org/10.1016/j.ajpath.2011.07.022.
[8] C. Saury, A. Lardenois, C. Schleder, I. Leroux, B. Lieubeau, L. David, M. Charrier, L. Guével, S. Viau, B. Delorme, K. Rouger, Human serum and platelet lysate are appropriate xeno-free alternatives for clinical-grade production of human MuStem cell batches, Stem Cell Res Ther 9 (2018), https://doi.org/10.1186/s13287-018-0852-y.
[9] A. Lardenois, S. Jagot, M. Lagarrigue, B. Guével, M. Ledevin, T. Larcher, L. Dubreil, C. Pineau, K. Rouger, L. Guével, Quantitative proteome profiling of dystrophic dog skeletal muscle reveals a stabilized muscular architecture and protection against oxidative stress after systemic delivery of MuStem cells, Proteomics 16 (2016) 2028–2042, https://doi.org/10.1002/pmic.201600002.

[10] A. Rannou, G. Toumaniantz, T. Larcher, I. Leroux, M. Ledevin, A. Hivonnait, C. Babarit, R. Fleurisson, L. Dubreil, S. Ménoret, I. Anegon, F. Charpentier, K. Rouger, L. Guével, Human MuStem cell grafting into infarcted rat heart attenuates adverse tissue remodeling and preserves cardiac function, Mol Ther Methods Clin Dev 18 (2020) 446–463, https://doi.org/10.1016/j.omtm.2020.06.009.
[11] F. Robriquet, A. Lardenois, C. Babarit, T. Larcher, L. Dubreil, I. Leroux, C. Zuber, M. Ledevin, J.Y. Deschamps, Y. Fromes, Y. Cherel, L. Guevel, K. Rouger, Differential gene expression profiling of dystrophic dog muscle after MuStem cell transplantation, PloS One 10 (2015), https://doi.org/10.1371/journal.pone.0123336.
[12] I. Asselin, J.T. Vilquin, J.P. Tremblay, B. Guérette, R. Roy, Lymphocyte infiltration following allo- and xenomyoblast transplantation in mdx mice, Muscle Nerve 18 (1995) 39–51, https://doi.org/10.1002/mus.880180107.
[13] S. Ansari, C. Chen, X. Xu, N. Annabi, H.H. Zadeh, B.M. Wu, A. Khademhosseini, S. Shi, A. Moshaverinia, Muscle tissue engineering using gingival mesenchymal stem cells encapsulated in alginate hydrogels containing multiple growth factors, Ann. Biomed. Eng. 44 (2016) 1908–1920, https://doi.org/10.1007/s10439-016-1594-6.
[14] D. Boso, E. Maghin, E. Carraro, M. Giagante, P. Pavan, M. Piccoli, Extracellular matrix-derived hydrogels as biomaterial for different skeletal muscle tissue replacements, Materials 13 (2020), https://doi.org/10.3390/ma13112483.
[15] D.E. Discher, D.J. Mooney, P.W. Zandstra, Growth factors, matrices, and forces combine and control stem cells, Science 324 (2009) (1979) 1673–1677, https://doi.org/10.1126/science.1171643.
[16] H. Kim, C. Bae, Y.M. Kook, W.G. Koh, K. Lee, M.H. Park, Mesenchymal stem cell 3D encapsulation technologies for biomimetic microenvironment in tissue regeneration, Stem Cell Res Ther 10 (2019), https://doi.org/10.1186/s13287-018-1130-8.
[17] K.H. Vining, D.J. Mooney, Mechanical forces direct stem cell behaviour in development and regeneration, Nat. Rev. Mol. Cell Biol. 18 (2017) 728–742, https://doi.org/10.1038/nrm.2017.108.
[18] S. Dupont, L. Morsut, M. Aragona, E. Enzo, S. Giulitti, M. Cordenonsi, F. Zanconato, J. Le Digabel, M. Forcato, S. Bicciato, N. Elvassore, S. Piccolo, Role of YAP/TAZ in mechanotransduction, Nature 474 (2011) 179–184, https://doi.org/10.1038/nature10137.
[19] M. Aragona, T. Panciera, A. Manfrin, S. Giulitti, F. Michielin, N. Elvassore, S. Dupont, S. Piccolo, A mechanical checkpoint controls multicellular growth through YAP/TAZ regulation by actin-processing factors, Cell 154 (2013) 1047–1059, https://doi.org/10.1016/j.cell.2013.07.042.
[20] A. Engler, L. Bacakova, C. Newman, A. Hategan, M. Griffin, D. Discher, Substrate compliance versus ligand density in cell on gel responses, Biophys. J. 86 (2004) 617–628, https://doi.org/10.1016/S0006-3495(04)74140-5.
[21] A.J. Capel, R.P. Rimington, J.W. Fleming, D.J. Player, L.A. Baker, M.C. Turner, J. M. Jones, N.R.W. Martin, R.A. Ferguson, V.C. Mudera, M.P. Lewis, Scalable 3D printed molds for human tissue engineered skeletal muscle, Front. Bioeng. Biotechnol. 7 (2019), https://doi.org/10.3389/fbioe.2019.00020.
[22] V. Hosseini, S. Ahadian, S. Ostrovidov, G. Camci-Unal, S. Chen, H. Kaji, M. Ramalingam, A. Khademhosseini, Engineered contractile skeletal muscle tissue on a microgrooved methacrylated gelatin substrate, Tissue Eng. Part A 18 (2012) 2453–2465, https://doi.org/10.1089/ten.tea.2012.0181.
[23] J. Kim, B.-K. Koo, J.A. Knoblich, Human organoids: model systems for human biology and medicine, Nat. Rev. Mol. Cell Biol. 21 (2020) 571–584, https://doi.org/10.1038/s41580-020-0259-3.
[24] J. Liu, H. Zheng, P.S.P. Poh, H.G. Machens, A.F. Schilling, Hydrogels for engineering of perfusable vascular networks, Int. J. Mol. Sci. 16 (2015) 15997–16016, https://doi.org/10.3390/ijms160715997.
[25] B.V. Slaughter, S.S. Khurshid, O.Z. Fisher, A. Khademhosseini, N.A. Peppas, Hydrogels in regenerative medicine, Adv. Mater. 21 (2009) 3307–3329, https://doi.org/10.1002/adma.200802106.
[26] B.A. Aguado, W. Mulyasasmita, J. Su, K.J. Lampe, S.C. Heilshorn, Improving viability of stem cells during syringe needle flow through the design of hydrogel cell carriers, Tissue Eng. Part A 18 (2012) 806–815, https://doi.org/10.1089/ten.tea.2011.0391.
[27] M.C. Darnell, J.-Y. Sun, M. Mehta, C. Johnson, P.R. Arany, Z. Suo, D.J. Mooney, Performance and biocompatibility of extremely tough alginate/polyacrylamide hydrogels, Biomaterials 34 (2013) 8042–8048, https://doi.org/10.1016/j.biomaterials.2013.06.061.
[28] K.Y. Lee, D.J. Mooney, Alginate: properties and biomedical applications, Prog. Polym. Sci. 37 (2012) 106–126, https://doi.org/10.1016/j.progpolymsci.2011.06.003.
[29] M.I. Neves, L. Moroni, C.C. Barrias, Modulating alginate hydrogels for improved biological performance as cellular 3D microenvironments, Front. Bioeng. Biotechnol. 8 (2020), https://doi.org/10.3389/fbioe.2020.00665.
[30] G.T. Grant, E.R. Morris, D.A. Rees, P.J.C. Smith, D. Thom, Biological interactions between polysaccharides and divalent cations: the egg-box model, FEBS Lett. 32 (1973) 195–198, https://doi.org/10.1016/0014-5793(73)80770-7.
[31] G. Kaklamani, D. Cheneler, L.M. Grover, M.J. Adams, J. Bowen, Mechanical properties of alginate hydrogels manufactured using external gelation, J. Mech. Behav. Biomed. Mater. 36 (2014) 135–142, https://doi.org/10.1016/j.jmbbm.2014.04.013.
[32] C. Liu, D. Lewin Mejia, B. Chiang, K.E. Luker, G.D. Luker, Hybrid collagen alginate hydrogel as a platform for 3D tumor spheroid invasion, Acta Biomater. 75 (2018) 213–225, https://doi.org/10.1016/j.actbio.2018.06.003.
[33] M. Mancini, M. Moresi, R. Rancini, Mechanical properties of alginate gels: empirical characterisation, J. Food Eng. 39 (1999) 369–378, https://doi.org/10.1016/S0260-8774(99)00022-9.
[34] P.M. Gilbert, K.L. Havenstrite, K.E.G. Magnusson, A. Sacco, N.A. Leonardi, P. Kraft, N.K. Nguyen, S. Thrun, M.P. Lutolf, H.M. Blau, Substrate elasticity regulates skeletal muscle stem cell self-renewal in culture, Science 329 (2010) (1979) 1078–1081, https://doi.org/10.1126/science.1191035.
[35] J.G. Jacot, J.C. Martin, D.L. Hunt, Mechanobiology of cardiomyocyte development, J. Biomech. 43 (2010) 93–98, https://doi.org/10.1016/j.jbiomech.2009.09.014.
[36] J. Jang, Y.J. Seol, H.J. Kim, J. Kundu, S.W. Kim, D.W. Cho, Effects of alginate hydrogel cross-linking density on mechanical and biological behaviors for tissue engineering, J. Mech. Behav. Biomed. Mater. 37 (2014) 69–77, https://doi.org/10.1016/j.jmbbm.2014.05.004.
[37] Ý.A. Mørch, I. Donati, B.L. Strand, G. Skjåk-Bræk, Effect of Ca2+, Ba2+, and Sr2+ on alginate microbeads, Biomacromolecules 7 (2006) 1471–1480, https://doi.org/10.1021/bm060010d.
[38] F. Seidi, M. Khodadadi Yazdi, M. Jouyandeh, M. Dominic, H. Naeim, M.N. Nezhad, B. Bagheri, S. Habibzadeh, P. Zarrintaj, M.R. Saeb, M. Mozafari, Chitosan-based blends for biomedical applications, Int. J. Biol. Macromol. 183 (2021) 1818–1850, https://doi.org/10.1016/j.ijbiomac.2021.05.003.
[39] K.R. Shoueir, N. El-Desouky, M.M. Rashad, M.K. Ahmed, I. Janowska, M. El-Kemary, Chitosan based-nanoparticles and nanocapsules: overview, physicochemical features, applications of a nanofibrous scaffold, and bioprinting, Int. J. Biol. Macromol. 167 (2021) 1176–1197, https://doi.org/10.1016/j.ijbiomac.2020.11.072.
[40] R. Karimi-Soflou, I. Shabani, A. Karkhaneh, Enhanced neural differentiation by applying electrical stimulation utilizing conductive and antioxidant alginate-polypyrrole/poly-l-lysine hydrogels, Int. J. Biol. Macromol. 237 (2023) 124063, https://doi.org/10.1016/j.ijbiomac.2023.124063.
[41] P. Tournier, G. Saint-Pé, N. Lagneau, F. Loll, B. Halgand, A. Tessier, J. Guicheux, C. Le Visage, V. Delplace, Clickable dynamic bioinks enable post-printing modifications of construct composition and mechanical properties controlled over time and space, Adv. Sci. 10 (2023), https://doi.org/10.1002/advs.202300055.
[42] A. Zykwinska, M. Marquis, M. Godin, L. Marchand, C. Sinquin, C. Garnier, C. Jonchère, C. Chédeville, C. Le Visage, J. Guicheux, S. Colliec-Jouault, S. Cuenot, Microcarriers based on glycosaminoglycan-like marine exopolysaccharide for TGF-β1 long-term protection, Mar. Drugs 17 (2019) 65, https://doi.org/10.3390/md17010065.
[43] S. Cuenot, P. Gélébart, C. Sinquin, S. Colliec-Jouault, A. Zykwinska, Mechanical relaxations of hydrogels governed by their physical or chemical crosslinks, J. Mech. Behav. Biomed. Mater. 133 (2022) 105343, https://doi.org/10.1016/j.jmbbm.2022.105343.
[44] H. Hertz, Ueber die Berührung fester elastischer Körper, Journal Für Die Reine Und Angewandte Mathematik 92 (1881) 156–171.
[45] A. Zykwinska, O. Makshakova, P. Gélébart, C. Sinquin, N. Stephant, S. Colliec-Jouault, S. Perez, S. Cuenot, Interactions between infernan and calcium: from the molecular level to the mechanical properties of microgels, Carbohydr. Polym. 292 (2022) 119629, https://doi.org/10.1016/j.carbpol.2022.119629.
[46] F. Hached, C. Vinatier, P.-G. Pinta, P. Hulin, C. Le Visage, P. Weiss, J. Guicheux, A. Billon-Chabaud, G. Grimandi, Polysaccharide hydrogels support the long-term viability of encapsulated human mesenchymal stem cells and their ability to secrete immunomodulatory factors, Stem Cells Int. 2017 (2017) 1–11, https://doi.org/10.1155/2017/9303598.
[47] F. Nativel, D. Renard, F. Hached, P.G. Pinta, C. D'Arros, P. Weiss, C. Le Visage, J. Guicheux, A. Billon-Chabaud, G. Grimandi, Application of millifluidics to encapsulate and support viable human mesenchymal stem cells in a polysaccharide hydrogel, Int. J. Mol. Sci. 19 (2018), https://doi.org/10.3390/ijms19071952.
[48] R.C. "Dutch" Boltz, P.A. Fischer, L.S. Wicker, L.B. Peterson, Single UV excitation of hoechst 33342 and ethidium bromide for simultaneous cell cycle analysis and viability determinations on in vitro cultures of murine B lymphocytes, Cytometry 15 (1994) 28–34, https://doi.org/10.1002/cyto.990150106.
[49] G. Talei Franzesi, B. Ni, Y. Ling, A. Khademhosseini, A controlled-release strategy for the generation of cross-linked hydrogel microstructures, J. Am. Chem. Soc. 128 (2006) 15064–15065, https://doi.org/10.1021/ja065867x.
[50] A. Sergeeva, A.S. Vikulina, D. Volodkin, Porous alginate scaffolds assembled using vaterite CaCO3 crystals, Micromachines (Basel) 10 (2019) 357, https://doi.org/10.3390/mi10060357.
[51] S. Swioklo, A. Constantinescu, C.J. Connon, Alginate-encapsulation for the improved hypothermic preservation of human adipose-derived stem cells, Stem Cells Transl. Med. 5 (2016) 339–349, https://doi.org/10.5966/sctm.2015-0131.
[52] S. Akbari, T. Pirbodaghi, Microfluidic encapsulation of cells in alginate particles via an improved internal gelation approach, Microfluid. Nanofluid. 16 (2014) 773–777, https://doi.org/10.1007/s10404-013-1264-z.
[53] A.S. Mao, J.-W. Shin, S. Utech, H. Wang, O. Uzun, W. Li, M. Cooper, Y. Hu, L. Zhang, D.A. Weitz, D.J. Mooney, Deterministic encapsulation of single cells in thin tunable microgels for niche modelling and therapeutic delivery, Nat. Mater. 16 (2017) 236–243, https://doi.org/10.1038/nmat4781.
[54] O. Chaudhuri, L. Gu, D. Klumpers, M. Darnell, S.A. Bencherif, J.C. Weaver, N. Huebsch, H. Lee, E. Lippens, G.N. Duda, D.J. Mooney, Hydrogels with tunable stress relaxation regulate stem cell fate and activity, Nat. Mater. 15 (2016) 326–334, https://doi.org/10.1038/nmat4489.
[55] Y. Maki, K. Ito, N. Hosoya, C. Yoneyama, K. Furusawa, T. Yamamoto, T. Dobashi, Y. Sugimoto, K. Wakabayashi, Anisotropic structure of calcium-induced alginate gels by optical and small-angle X-ray scattering measurements, Biomacromolecules 12 (2011) 2145–2152, https://doi.org/10.1021/bm200223p.

[56] A. Maire du Poset, A. Lerbret, A. Zitolo, F. Cousin, A. Assifaoui, Design of polygalacturonate hydrogels using iron(II) as cross-linkers: a promising route to protect bioavailable iron against oxidation, Carbohydr. Polym. 188 (2018) 276–283, https://doi.org/10.1016/j.carbpol.2018.02.007.
[57] A. Maire Du Poset, A. Lerbret, F. Boué, A. Zitolo, A. Assifaoui, F. Cousin, Tuning the structure of galacturonate hydrogels: external gelation by Ca, Zn, or Fe cationic cross-linkers, Biomacromolecules 20 (2019) 2864–2872, https://doi.org/10.1021/acs.biomac.9b00726.
[58] X. Lin, J. Shi, G. Meng, C. Yu, Sodium alginate hydrogel carrier with calcium carbonate as calcium source for ibuprofen release, Macromol. Chem. Phys. 224 (2023), https://doi.org/10.1002/macp.202300195.
[59] A. Bozza, E.E. Coates, T. Incitti, K.M. Ferlin, A. Messina, E. Menna, Y. Bozzi, J. P. Fisher, S. Casarosa, Neural differentiation of pluripotent cells in 3D alginate-based cultures, Biomaterials 35 (2014) 4636–4645, https://doi.org/10.1016/j.biomaterials.2014.02.039.
[60] L. Li, Y. Chen, Y. Wang, F. Shi, Y. Nie, T. Liu, K. Song, Effects of concentration variation on the physical properties of alginate-based substrates and cell behavior in culture, Int. J. Biol. Macromol. 128 (2019) 184–195, https://doi.org/10.1016/j.ijbiomac.2019.01.123.
[61] M. Leijs, E. Villafuertes, J. Haeck, W. Koevoet, B. Fernandez-Gutierrez, M. Hoogduijn, J. Verhaar, M. Bernsen, G. van Buul, G. van Osch, Encapsulation of allogeneic mesenchymal stem cells in alginate extends local presence and therapeutic function, Eur. Cell. Mater. 33 (2017) 43–58, https://doi.org/10.22203/eCM.v033a04.